ELSEVIER

Thermochimica Acta 282/283 (1996) 277–296

thermochimica acta

# A study of calcium oxalate monohydrate using dynamic differential scanning calorimetry and other thermoanalytical techniques[1]

Keith J. Kociba[a], Patrick K. Gallagher[a,b]

[a] *Department of Chemistry, The Ohio State University, Columbus, OH 43210-1173, USA*

[b] *Department of Materials Science, The Ohio State University, Columbus, OH 43210-1173, USA*

**Abstract**

The focus of this work is the characterization of the order–disorder phase transition of calcium oxalate monohydrate. MDSC™, power-compensated DSC, EGA/MS, XRD, TG, and TMA were utilized to investigate the reproducibility, reversibility, and heating rate dependence of this transition. Flowing atmospheres saturated with water vapor were used to shift the dehydration equilibrium to a higher temperature so as to better resolve the order–disorder phase transition from the dehydration. Differences in thermal behavior of the sample due to the use of open versus semi-closed sample pans were also investigated. Correlations were made with spectroscopic (Raman, DRIFTS/MS, IR emission) and XRD results from the literature. This article reports the first MDSC™, DSC and TMA results for the order–disorder phase transition of $CaC_2O_4 \cdot H_2O$.

*Keywords:* Dynamic differential scanning calorimetry; Thermoanalytical techniques; Calcium oxalate monohydrate

## 1. Introduction

Calcium oxalate monohydrate, $CaC_2O_4 \cdot H_2O$, undergoes dehydration, decomposition to $CaCO_3$ and further decomposition to CaO in an easily accessible temperature range (ambient to 800°C). Less well-known concerning $CaC_2O_4 \cdot H_2O$ is that it exists in

* Corresponding author.

[1] Dedicated to Takeo Ozawa on the Occasion of his 65th Birthday.


*SSDI* 0040-6031(95)02812-2

two phases, known as the low-temperature and high-temperature phases, according to Raman and IR emission spectroscopies [1,2]. The Joint Committee for Powder Diffraction Standards (JCPDS) reports not two, but five different phases of the monohydrate according to XRD results [3–5]. Coexistence of the low- and high-temperature phases was noted in both Raman and XRD results [1,6]. Completion of the low- to high-temperature phase transition occurs between 45 and 50°C according to the results of Raman [1], XRD [7], and (indirectly) by diffuse reflectance infrared fourier transform spectroscopy (DRIFTS) [8]. See Table 1 for a summary of the thermal behavior of calcium oxalate monohydrate. See Table 2 for a compilation of literature results regarding characterization of the thermal behavior of calcium oxalate monohydrate from subambient to 100°C using many analytical techniques. Literature results in this regard for calcium oxalate monohydrate and subsequent products from subambient to 900°C are presented in similar form in Ref. [19].

MDSC™, power-compensated DSC and XRD were the primary investigative tools in this work, with EGA/MS, TG, and TMA serving as complementary methods. MDSC™, or dynamic DSC, is a relatively new thermoanalytical technique described elsewhere [20–22]. This work demonstrates the sensitivity of MDSC™ to subtle and/or higher-order transitions and the advantages of continuous specific heat capacity measurement.

Table 1
Thermal behavior of calcium oxalate monohydrate

| Approximate temperature/°C | Transition or behavior (according to reference authors) |
|---|---|
| −197[a] | All $CaC_2O_4 \cdot H_2O$ exists only as $CaC_2O_4 \cdot H_2O$(I) |
| Unknown | $CaC_2O_4 \cdot H_2O$(II) begins to form from $CaC_2O_4 \cdot H_2O$(I) |
| < 20[a,b] | $CaC_2O_4 \cdot H_2O$(II) coexists with $CaC_2O_4 \cdot H_2O$(I) |
| 45–50[c,d] | All remaining $CaC_2O_4 \cdot H_2O$(I) converted to $CaC_2O_4 \cdot H_2O$(II) (upper temperature limit of form (I)'s existence) |
| 200[d–h] | $CaC_2O_4 \cdot H_2O \leftrightarrow \alpha\text{-}CaC_2O_4 + H_2O$ |
| 230[c,d,h–j,l] | $\alpha\text{-}CaC_2O_4 \leftrightarrow \beta\text{-}CaC_2O_4$ |
| 350–400[c,j–l] | $\beta\text{-}CaC_2O_4 \leftrightarrow \gamma\text{-}CaC_2O_4$ |
| > 400[k–m] | $CaC_2O_4 \leftrightarrow CaCO_3$ (calcite) + CO |

$CaC_2O_4 \cdot H_2O$(I) P21/*n* ($C^5_{2h}$), low-temperature form.
$CaC_2O_4 \cdot H_2O$(II) I2/*m* ($C^3_{2h}$), high-temperature form.
[a] Ref. [1]. [b] Ref. [6]. [c] Ref. [8]. [d] Ref. [9]. [e] Ref. [10]. [f] Ref. [2] [g] Ref. [11].
[h] Ref. [12]. [i] Ref. [13]. [j] Ref. [14]. [k] Ref. [15]. [l] Ref. [16]. [m] Ref. [17].

Table 2
Summary, as a function of increasing onset temperature, of the major and relevant minor results for the analyses of calcium oxalate monohydrate performed to date using various analytical techniques. Experimental conditions (unless otherwise noted) were ambient pressure, air atmosphere, open sample holders, and no control of the partial pressure of water. Note: The conclusions and speculations listed here are those proposed by the author(s) of the listed reference.

| Temperature/°C | Method | Observation | Conclusion or speculation |
|---|---|---|---|
| All | TG[a] | Effects of sample mass on TG results | $H_2O$ and CO evolution are rate-controlled by phase boundary reactions |
| − 197 | Raman[b] | No evidence of the high-temperature phase of $CaC_2O_4 \cdot H_2O$ | High-temperature phase does not persist to very low temperatures |
| − 197 to 131 | Raman[b] | No bands observed above 1800 $cm^{-1}$ in the spectra | |
| > − 50 (heating) | Calorimetry[c] | Specific heat capacity curve becomes rough, losing its previously smooth profile | |
| Sub-ambient | Spectroscopy in general[b] | | No evidence for other phase transitions |
| 20 | XRD[d] | Two distinct calcium sites and two non-equivalent, nearly orthogonal oxalate groups in the crystal structure | High- and low-temperature forms of $CaC_2O_4 \cdot H_2O$ coexist at room temperature |
| Room temperature | XRD[b] | Starting material pattern matches JCPDS file 20–231 except for a weak peak at $d = 4.76$ Å which matches the high-temperature phase XRD pattern | Coexistence of the basic and derivative structures of $CaC_2O_4 \cdot H_2O$ |
| Room temperature | Raman[e] | Raman bands at 210°C, known to belong to α-$CaC_2O_4$, match those of anhydrous $CaC_2O_4$ at room temperature | α-$CaC_2O_4$ is the stable form of anhydrous calcium oxalate at room temperature |
| Ambient, after heating to 500°C | DRIFTS/MS[f] | Sample color was gray (white at start) | Empirical confirmation of disproportionation of CO product, C |
| 22 | Raman[b] | Weak band appears at 322 $cm^{-1}$; this band decreases continuously in wavenumber as sample is cooled | Raman-active component of $\nu'_8$ |
| 22 | XRD[g] | 182 (out of 2321) reflections with $k$ odd are present, but intensities are weak | Unequivocal support of a value of $b = 14.60(3)$ Å |

Table 2 (Continued)

| Temperature/°C | Method | Observation | Conclusion or speculation |
|---|---|---|---|
| 38 | XRD[g] | Just the most intense superstructure reflections can be recorded | Onset of the transition from derivative ($P2_1/n$) to basic ($I2/m$) structure |
| < 45 (upon heating) | Raman[b] | Rayleigh line broadens faster near the transition temperature | Domains of the high-temperature phase precipitate around edge dislocations |
| 45 | Raman[b] | Discontinuity in the wave numbers assigned to two fundamentals of the oxalate rotatory motions on either side of the transition temperature | Indicates first-order kinetics for the transformation because higher-order phase transitions show no discontinuity in $\Delta G$ as the temperature is decreased through the transition temperature; hence, no discontinuity possible without first-order kinetics |
| 45 | Raman[b] | | Data verify the order–disorder ($P2_1/n$–$I2/m$) polymorphic phase transition and that the two phases coexist between 0 and 131°C |
| 45 ± | Raman[b] | Most low wave number bands and higher wave number rotatory motions of the structural water units tend to damp | Domain formation induces directional stress and dampens phonons as the $k = 0$ selection rule breaks down for phonons whose wave vectors do not coincide with the direction of the distortion |
| 45 (upon cooling) | XRD[g] | Superstructure reflections reappear | Ordering takes place; transition from derivative ($P2_1/n$) to basic ($I2/m$) structure is reversible |
| > 45 (upon cooling) | Raman[b] | Rayleigh line appears to broaden slowly as transition temperature approached | Low-temperature phase precipitates at point defects |
| 45–152 | XRD[g] | No changes in XRD pattern | No other structural change occurs |
| 50–100 | DRIFTS/MS[h] | Band at 1625 $cm^{-1}$ shifts to higher frequency | Result of loss of water from the crystal lattice |
| 55 | XRD[g] | All reflections with $k$ odd disappear; the value of the $b$ translation is one-half that of room temperature | Transition from derivative ($P2_1/n$) to basic ($I2/m$) structure |
| > 100 | DRIFTS/MS[c] | 1627, 1319, and 781 $cm^{-1}$ bands shift to higher wavenumbers | Onset of dehydration; loss of water from crystal results in larger stretching and bending force constants for oxalate anions |

Table 2 (Continued)

| Temperature/°C | Method | Observation | Conclusion or speculation |
|---|---|---|---|
| 100 | DRIFTS/MS[f] | New band at 1660 $cm^{-1}$ appears | Combination band; probably originates from same source as 1709 $cm^{-1}$ band reported by Shippey [2] for IR spectrum of $\beta$-$CaC_2O_4$ |
| 100 | IR[i] | Band at 1709 $cm^{-1}$ appears | Combination band; low-frequency oxalate anion rotatory motion; may be masked by intense $\nu_9$ absorption in the monohydrate |

[a] Ref. [18]. [b] Ref. [1]. [c] Ref. [24]. [d] Ref. [6]. [e] Ref. [14]. [f] Ref. [8]. [g] Ref. [7]. [h] Ref. [9]. [i] Ref. [2].

## 2. Experimental section

ACS reagent grade $CaC_2O_4 \cdot H_2O$ was used. The sample was stored in a twist-cap vial exposed to normal room temperatures and atmospheric conditions. All experiments used this sample as received.

Dynamic DSC experiments were performed using a TA Instruments Model 2910 and, later, a Model 2920 heat-flux cell design MDSC™. Temperature, enthalpy and the specific heat capacity constant were all calibrated according to manufacturer specifications. Cyclohexane, indium, tin, lead and zinc were the temperature standards; indium, tin, lead and zinc were the enthalpy standards and a 60-mg single-crystal sapphire was the standard for specific heat capacity.

Calcium oxalate monohydrate samples of various masses were placed in the manufacturer's aluminium sample pans. The masses of the sample and reference pans for any given experiment were always matched to within 0.05 mg. The lids of these sample pans, when used, were pressed firmly into the bottoms, but not crimped, using a die press from TA Instruments. This was to ensure good thermal contact of the sample with the pan bottom and simultaneously to allow escape of the gaseous decomposition products.

The atmosphere in the MDSC™ cell was 99.998% pure dry nitrogen flowing at 50 ml $min^{-1}$. The vacuum line of the MDSC™ was continuously purged with approximately 50 ml $min^{-1}$ industrial grade dry nitrogen. Some experiments utilized an atmosphere of nitrogen saturated with water vapor. This consisted of the same gases and flow rates, but with the in-line addition of a fritted glass bubbler submerged no less than 3 inches below the surface of an approximately half-full distilled water reservoir left standing at room temperature.

Power-compensated DSC experiments were performed using a Perkin-Elmer DSC7. Twenty-milligram samples of calcium oxalate monohydrate were placed in the same sample pans as used in the MDSC™ experiments. Masses of the sample pans were again matched to within 0.05 mg, and lids, which were always used, were placed in the

same manner as in the MDSC™ experiments. The atmosphere in the DSC cell was stagnant 99.998% pure nitrogen. Temperature was calibrated using the melting point of cyclohexane. Enthalpy was calibrated using indium.

Thermogravimetric analyses were conducted using a Model 951 TGA from TA Instruments. Determinations of calcium oxalate monohydrate purity utilized 5-mg samples in platinum hanging-type boats heated at 5°C $min^{-1}$ in a 99.998% pure dry nitrogen atmosphere flowing at 30 ml $min^{-1}$.

A Scintag XDS 2000 variable-temperature heated-stage XRD was used to acquire all XRD patterns. Copper K$\alpha$ X-rays ($\lambda = 1.54060$ Å) were used in all experiments. The $2\theta$ scan rate was 2° $min^{-1}$ in all experiments, except for analyses of starting material in which case the scan rate was 1° $min^{-1}$. XRD patterns were acquired in a continuous-scan mode with a step size of 0.03° and dwell time of 0.90 s for the 2° $min^{-1}$ scans (1.8 s for 1° $min^{-1}$ scans). All patterns were acquired isothermally $\pm$ 1°C at the temperatures indicated on the plots. The atmosphere always consisted of 99.998% argon flowing at 20 ml $min^{-1}$ and was sometimes saturated with water vapor in the same manner as in the MDSC™ experiments. The stage was heated as quickly as possible to the target temperature and then held isothermally for ten minutes prior to the start of pattern acquisition. Overshoot of the target temperature was consistently < 7°C, and the target temperature was re-established less than 10 s after overshoot occurred.

A TA Instruments Model 943 TMA was used to study a 20 mg sample of calcium oxalate monohydrate loosely packed into an aluminium MDSC™ sample pan and heated at 1°C $min^{-1}$ from ambient temperature to 500°C in a furnace open to ambient atmospheric conditions. The expansion probe with a 1.0 g load was used. Temperature was calibrated using the melting points of indium and lead. $\Delta L/L$ was not calibrated.

Evolved gas analysis (EGA) was performed using a home-built UHV chamber housing a high-temperature furnace with programmer/controller (Leeds & Northrup) and a quadrupole mass spectrometer (United Technologies, Inc.) evacuated by a Balzers turbomolecular pump. System pressure ranged from $1 \times 10^{-6}$ to $8 \times 10^{-6}$ torr. Two-milligram samples of calcium oxalate monohydrate in clean, dry alumina crucibles were heated at 20°C $min^{-1}$ from 60 to 800°C. Ionizing electron energy was 70 eV and emission current was 2.45 mA.

## 3. Results and discussion

Purity of the starting material was verified by performing TG, XRD and EGA/MS analyses. The TG results in Fig. 1 show that the $CaC_2O_4 \cdot H_2O$ was stoichiometrically pure. An XRD pattern of the starting material (see Fig. 2) showed good agreement with the reference XRD pattern for the low-temperature form of calcium oxalate monohydrate [3] (JCPDS card 20–231). EGA/MS results (see Fig. 3) showed that no detectable quantities of species other than the expected decomposition products—$H_2O$ ($m/z = 18$), CO ($m/z = 28$), $CO_2$ ($m/z = 44$) and their cracking fragments—were evolved by the sample upon heating to 800°C. These results indicated that no volatile impurities were present in the starting material. The $m/z = 18$ peak was present with varying intensity throughout the duration of the experiment. The peak from 60 to 80°C was

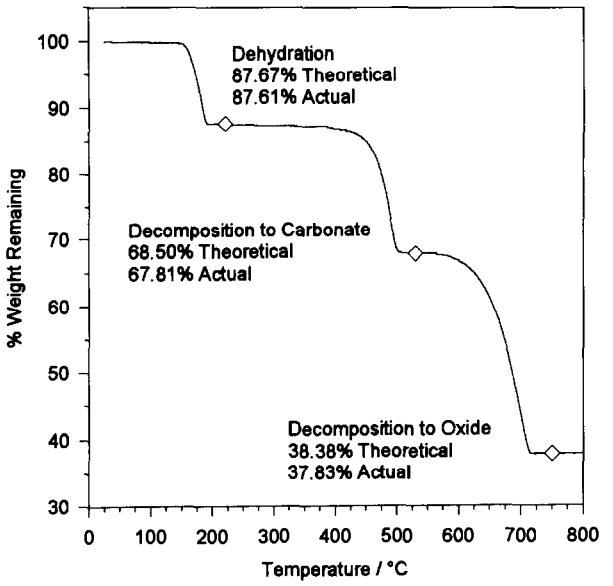


Fig. 1. Purity determination of starting material. TG results for 5.625 mg of calcium oxalate monohydrate heated at 5°C $min^{-1}$ in dry nitrogen flowing at 30 ml $min^{-1}$.

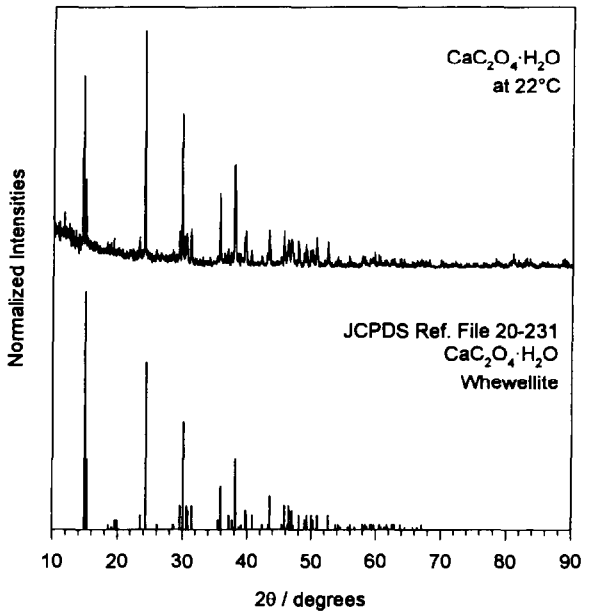


Fig. 2. XRD pattern of as-received calcium oxalate monohydrate compared to the literature XRD pattern for the low-temperature form of the monohydrate, JCPDS Reference File 20–231. Pattern acquired isothermally at 22°C in a stagnant air atmosphere with a $2\theta$ scan rate of 1° $min^{-1}$.

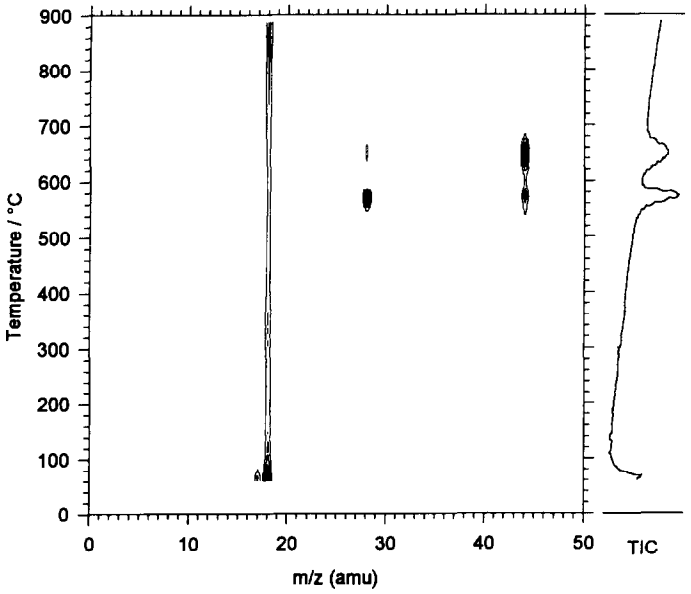


Fig. 3. EGA/MS results for 1.83 mg of calcium oxalate monohydrate heated at 20°C $min^{-1}$ in vacuum ($< 8 \times 10^{-6}$ Torr) in an alumina crucible. (TIC = total ion current at the detector.) Each contour represents a 5% signal intensity change.

caused by dehydration of the sample; the persistent $m/z = 18$ peak observed at higher temperatures was mostly background water which desorbed from surfaces inside the mass spectrometer. Also note that during the decomposition of calcium oxalate to calcium carbonate from 540 to 580°C, the product gas carbon monoxide ($m/z = 28$) underwent substantial disproportionation to carbon dioxide ($m/z = 44$). Accompanying the evolution of carbon dioxide at higher temperatures from the decomposition of calcium carbonate to calcium oxide was a peak at $m/z = 28$. This peak was a cracking fragment of carbon dioxide.

Preliminary MDSC™ experiments using $CaC_2O_4 \cdot H_2O$ were performed using a heating rate of 2°C $min^{-1}$ with a temperature modulation of ± 0.40°C every 30 s (2°C $min^{-1}$ ± 0.40°C per 30 s). All other figures show results obtained using a standard heating rate of 1°C $min^{-1}$ ± 1.00°C per 90 s. The slower heating rate, larger temperature amplitude and longer modulation period afforded increased sensitivity [23].

Fig. 4 compares MDSC™ results for calcium oxalate monohydrate in open aluminum sample pans heated at 2°C $min^{-1}$ ± 0.40°C per 30 s under nitrogen atmospheres both dry and saturated with water vapor. The presence of the water vapor clearly shifted the onset temperature of dehydration upward to 150°C. Dehydration under dry flowing nitrogen began near 85°C and was much broader. Fig. 5 shows the similarity of MDSC™ results under identical experimental conditions except for the use of a heating rate of 1°C $min^{-1}$ ± 1.00°C per 90 s instead of 2°C $min^{-1}$ ± 0.40°C per 30 s.

Fig. 5 also shows the effects of pan type and atmosphere on the MDSC™ results. Dehydration began at the lowest temperatures for the sample in an open pan under

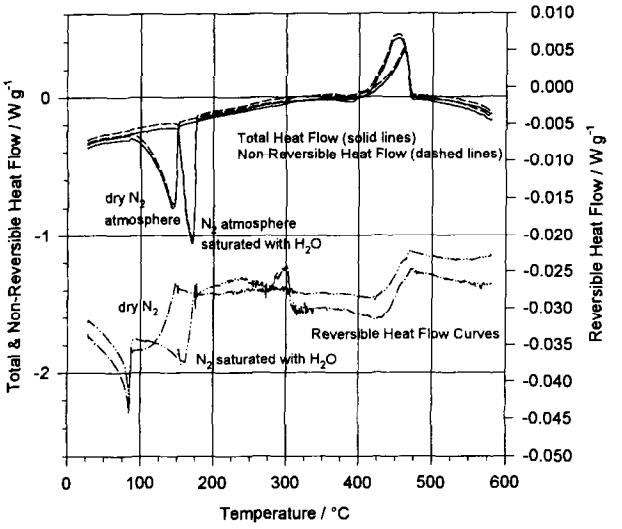


Fig. 4. MDSC™ results for calcium oxalate monohydrate heated at 2°C $min^{-1}$ ±0.40°C per 30 s in open aluminum sample pans under atmospheres of dry nitrogen and nitrogen saturated with water vapor.

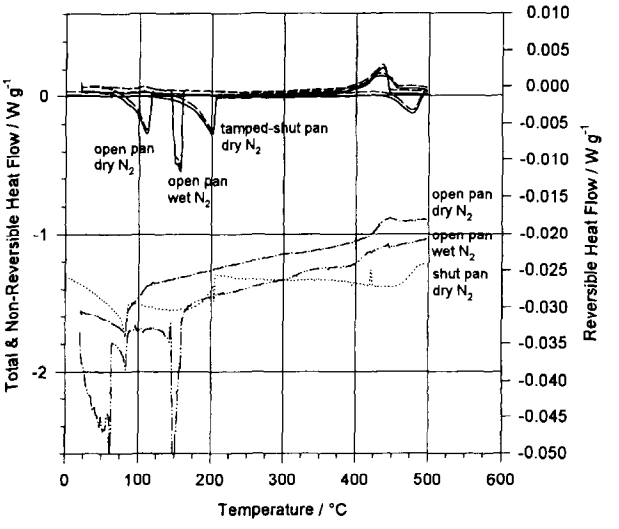


Fig. 5. MDSC™ results for calcium oxalate monohydrate heated at 1°C $min^{-1}$ ±1.00°C per 90 s in semicrimped and open aluminum sample pans under atmospheres of dry nitrogen and nitrogen saturated with water vapor.

a dry nitrogen atmosphere, followed by the sample in an open pan under an atmosphere saturated with water vapor. The sample in a covered but not crimped sample pan shows that the onset of dehydration occurred as low as 100°C, but the majority of the process did not occur until above 150°C due to the restricted exit of the product gas, which caused the equilibrium to shift to higher temperatures.

The reversible heat flow curves in Fig. 5, shown below the series of curves vertically centered about 0.0 W $g^{-1}$, reflected the behavior of the total heat flow curves. Large baseline shifts in the reversible heat flow curves correspond to dehydration in the total heat flow curves; the temperatures at which these shifts occur clearly show which reversible curve belongs to which set of experimental conditions. Note that the reversible curve for the experiment with the atmosphere saturated with water vapor exhibited a peak rather than a baseline shift during dehydration, in contrast to the results in Fig. 4. This curve also exhibited erratic behavior below 70°C, but that was due to the buildup of ice in the heat exchanger of the MDSC™ cell. The peak maximum belonging to the transition at 83°C did not shift as a function of pan type or atmospheric conditions.

Reproducibility of the transition at 83°C was proven by the results in Fig. 6. The total, non-reversible and reversible heat flow curves from independent experiments using fresh samples in open pans all under a dry flowing nitrogen atmosphere are shown. The total heat flow curves had a noticeable sinusoidal component which made accurate integration of the peak at 83°C impossible. The accuracy of the specific heat capacity calibration, which ultimately determines the separation of reversible from the total heat flow curve, was verified as correct by this set of experiments. The non-reversible heat flow curve showed nothing more than a ripple where the total and reversible curves exhibit peaks. Non-reversible heat flow profiles such as this indicate complete and accurate separation of the reversing component from the total heat flow. Finally, the peak maxima and enthalpies of the reversible heat flow peak were in excellent agreement, showing a high degree of reproducibility (see Table 3). The enthalpies and peak maxima of the transitions at 83°C from all MDSC™ experiments are presented in Table 4 along with the results from conventional DSC experiments.

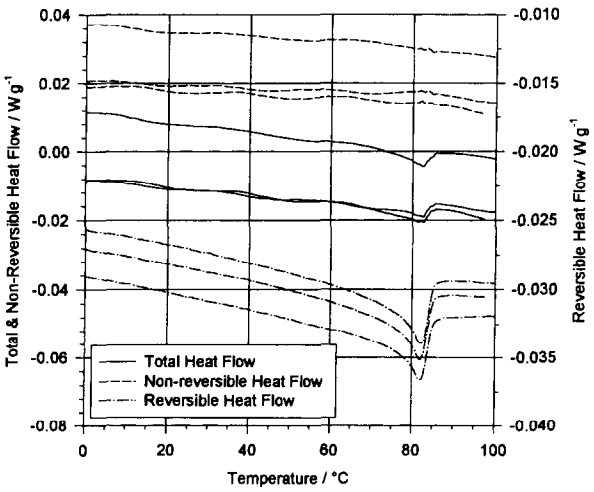


Fig. 6. Reproducibility of MDSC™ results (total, non-reversible and reversible heat flow curves) from an independent set of experiments using fresh samples in open pans all under a dry flowing nitrogen atmosphere with a heating rate of 1°C $min^{-1}$ ± 1.00°C per 90 s.

Unequivocal proof was obtained that the transition at 83°C belonged to the monohydrate form rather than the anhydrous form of calcium oxalate. A sample of as-received calcium oxalate monohydrate in a crimped pan was heated in the MDSC™ to 225°C under a dry nitrogen atmosphere to effect complete dehydration (confirmed by the DSC total heat flow curve's return to baseline after the dehydration peak). The sample was then cooled to 30°C. A second experiment repeated this procedure except that the sample was placed in an open pan and a nitrogen atmosphere saturated with water vapor was used. The resulting reversible heat flow profiles are shown in Fig. 7. Both curves exhibited the transition at 83°C upon heating, but only the curve from the experiment using an atmosphere saturated with water vapor exhibited this transition upon cooling, along with rehydration of the sample which was clearly observed as a separate event. The sample in the crimped pan clearly did not rehydrate and the transition at 83°C was completely absent upon cooling.

Table 3
Peak maxima and enthalpies of the transition at 83°C appearing in the reversible heat flow of Fig. 6. Experimental conditions: open sample pans and a heating rate of 1°C $min^{-1}$ ± 1.00°C/90 s. Range of integration: 30–95°C. Type of integration: four-point sigmoidal baseline

| Trial number | MDSC™ peak maximum/°C | MDSC™ $\Delta H$/(J $g^{-1}$) 30–95°C range |
|---|---|---|
| 1 | 81.94 | 2.696 |
| 2 | 81.92 | 2.633 |
| 3 | 81.53 | 2.676 |
| Average: | 81.66 ± 0.22 | 2.668 ± 0.03 |

Table 4
Peak maxima and enthalpies of the transition at 83°C appearing in the reversible heat flow of all MDSC™ experiments using calcium oxalate monohydrate in semi-closed sample pans and heating rates of 1°C $min^{-1}$ ± 1.00°C/90 s. Also shown are the peak maxima and enthalpies of the transition occurring between 65 and 80°C in conventional DSC experiments which also used samples in semi-closed pans and linear heating rates as listed. Range of integration: 30–95°C. Type of integration: four-point sigmoidal baseline

| Trial number | MDSC™ peak maximum/°C | MDSC™ $\Delta H$/(J $g^{-1}$) 30–95°C range | DSC heating rate/°C $min^{-1}$ | DSC peak maximum/°C | DSC $\Delta H$/(J $g^{-1}$) 30–95°C range |
|---|---|---|---|---|---|
| 1 | 82.57 | 2.758 | 1 | 58.35 | 9.337 |
| 2 | 82.54 | 1.337 | 2 | 74.55 | 3.976 |
| 3 | 82.78 | Immeasureable | 5 | 69.1 | 2.636 |
| 4 | 82.21 | 2.647 | 10 | 77.27 | 2.991 |
| 5 | 83.09 | 2.366 | 20 | 72.87 | 2.850 |
| 6 | 82.85 | 2.216 | | | |
| 7 | 83.25 | 2.961 | | | |
| Average: | 82.76 ± 0.33 | 2.381 ± 0.53 | – | – | 4.358 ± 2.53 |

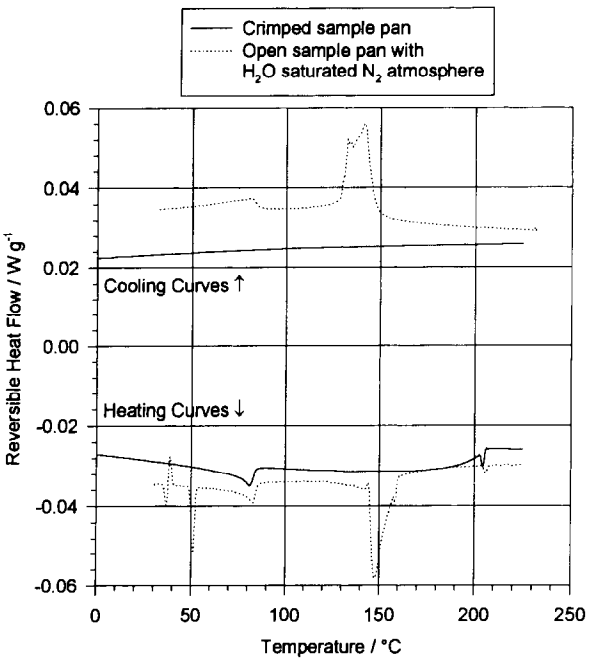


Fig. 7. Reversible heat flow curves from two MDSC™ experiments, one using dry nitrogen, the other using nitrogen saturated with water vapor, which prove that calcium oxalate is in the hydrated form when it undergoes the transition at 83°C. The small, reproducible endothermic peak at 205°C exhibited by both samples upon or near completion of dehydration is unexplained at present.

Fig. 8 shows that the transition which exhibited a peak at 83°C had an indeterminate onset temperature owing to the smooth curved baseline from −100 to 83°C. Once again the reversible heat flow profiles exhibited a high degree of reproducibility, and an unexpected result as well. A very small but reproducible endothermic peak occurred between −130 and −110°C in the three experiments with an initial temperature lower than −110°C. The maximum magnitude of this peak appeared to occur at a temperature related to the lowest temperature that the sample experienced. All of the experiments in which the samples experienced initial temperatures of less than −110°C exhibited nearly superimposable reversible heat flow profiles, but the single experiment in which the sample was not cooled to below −110°C exhibited a reversible heat flow profile which crossed over each of the other heat flow curves.

Fig. 9 shows the same data as Fig. 8 but as specific heat capacity values rather than reversible heat flow values. This allows comparison of the specific heat capacity curve from the literature [24] with the experimental results presented here. An anomolous bump at −150°C in the literature curve could represent the lower temperature limit of the endothermic peak observed to shift according to lowest temperature experienced by the sample. An inflection point and subsequent unexplained roughness in the literature values occurred around −70°C; no noticeable changes in the MDSC™

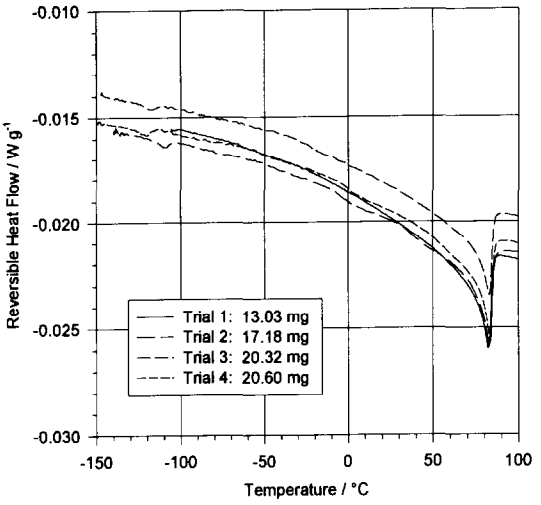


Fig. 8. MDSC™ reversible heat flow curves from four independent experiments heating calcium oxalate monohydrate in closed aluminum sample pans at 1°C $min^{-1}$ ± 1.0°C per 90 s in the −150°C to +100°C range.

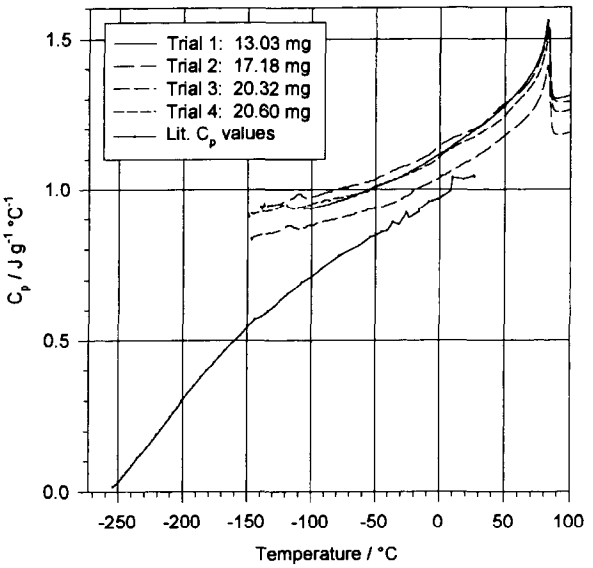


Fig. 9. MDSC™ specific heat capacity results from four independent experiments heating calcium oxalate monohydrate in closed aluminum sample pans at 1°C $min^{-1}$ ± 1.0°C per 90 s in the −150°C to +100°C range. These results are compared to literature values for the specific heat capacity of calcium oxalate monohydrate.

specific heat capacity curves occurred at these temperatures. The literature has made no mention of the temperature at which the low- and high-temperature phases of calcium oxalate monohydrate begin to coexist. A threshold temperature must exist, however, because the literature also cites that at −197°C no signs of the high-temperature form are present [1]. Thus the region between −110 and −70°C may well be that threshold.

The endothermic peak observed at 83°C in MDSC™ experiments at 1°C $min^{-1}$ was not observed in the conventional DSC experiments performed at 1°C $min^{-1}$. This seems contradictory, since MDSC™ total heat flow results are supposedly equivalent to conventional DSC results [20]. The explanation lies in the differences in instantaneous heating rate ($dT/dt$) experienced by samples in DSC and MDSC™ experiments, see Eqs. (1)–(4).

$$\text{DSC cell temperature algorithm} \quad T = T_0 + qt \tag{1}$$

$$\text{Instantaneous heating rate in DSC} \quad dT/dt = q \tag{2}$$

$$\text{MDSC}^{\text{TM}}\text{ cell temperature algorithm} \quad T = T_0 + qt + A_{T_b}\sin(\omega t) \tag{3}$$

$$\text{Instantaneous heating rate in MDSC}^{\text{TM}} \quad dT/dt = q + A_{T_b}\omega\cos(\omega t) \tag{4}$$

Where $T$ = cell temperature, $T_0$ = initial cell temperature, $q$ = programmed (or underlying) heating rate, $t$ = time, $A_{T_b}$ = amplitude of temperature modulation, $\omega = 2\pi/P$ = frequency of temperature modulation, $P$ = period of temperature modulation.

According to Eq. (4), the instantaneous heating rate in MDSC™ is not a constant as in DSC, but rather a function of time. The magnitude of the instantaneous heating rate depends on the amplitude and frequency of the temperature modulation. An MDSC™ thermal program of 1°C $min^{-1}$ ± 1.0°C per 90 s results in a maximum instantaneous heating rate of 5.2°C $min^{-1}$ and a minimum of −3.2°C $min^{-1}$. At 5°C $min^{-1}$, the monohydrate transition is clearly discernible by conventional DSC, thus its appearance in the reversible heat flow profile of the MDSC™ results is not surprising. This is an advantage of MDSC™ in that while slow underlying heating rates may be used to resolve proximate thermal events, thermodynamically higher-order thermal events which almost disappear at slower heating rates are still observed owing to the higher instantaneous heating rates experienced as a result of temperature modulation.

The peak height of the endothermic event observed by DSC in the 65–85°C range increased dramatically with increased heating rate. This result was not surprising since faster heating rates result in sharper peaks with greater displacement from baseline in differential experimental methods. The enthalpy of the phase transition should not change as a function of heating rate because enthalpy is a thermodynamic state function. Note the agreement among the enthalpies listed in Table 4 with the restriction of heating rates ≥ 5°C $min^{-1}$ for DSC results.

The broad and ill-defined onsets of the peaks observed in Fig. 10 indicate that the phase transition is not first-order in the thermodynamic sense. Thermodynamics formally defines first- and higher-order transitions as follows: if the Gibbs free energy function is discontinuous at the transformation temperature, it is a first-order trans-

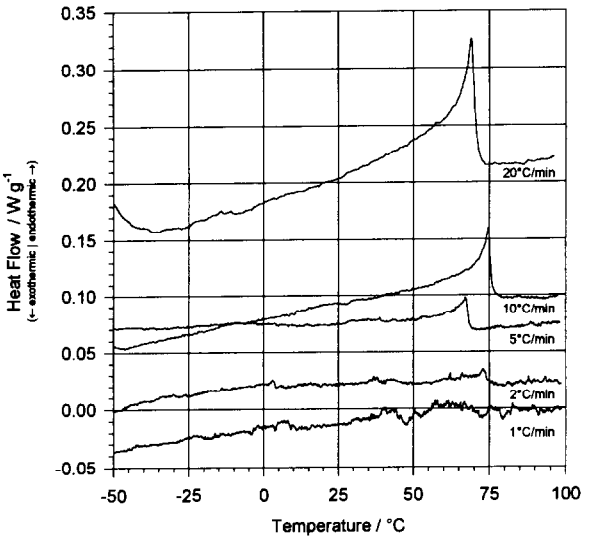


Fig. 10. Effects of heating rate on the power-compensated DSC heat flow profiles of calcium oxalate monohydrate in the − 50°C to 100°C region.

formation; if not, it is of higher order [25]. Higher-order transitions show little or no structural alterations [25]. The thermal event observed between 65 and 83°C by DSC and MDSC™ meets this latter criterion, if this event is indeed the order–disorder transition previously observed at 45–50°C [1, 7, 8].

The DSC heat flow curves and MDSC™ reversible heat flow curves both clearly exhibit a "lambda"-type curve shape. They also exhibit an accelerated increase in heat capacity as the critical temperature (approximately 80°C) is approached. (Recall that the reversible heat flow in MDSC™ reflects the specific heat capacity of the sample.) Thus it seems likely that the thermal event observed here is a higher-order lambda transition with respect to thermodynamics. This is not in contradiction with the first-order nature of the kinetics of the order–disorder transition at 45°C described by Duval and Condrate [1] in accordance with the results of Raman spectroscopy experiments: the orders of an event with respect to kinetics and thermodynamics are unrelated.

The 45–50°C regions of the DSC and MDSC™ experiments were unexpectedly featureless. Previous results [1, 7, 8] had shown this to be the low- to high-temperature transition region. Differences in experimental conditions may partly explain this discrepancy. The DRIFTS/MS experiments used samples of 0.96% (wt/wt) $CaC_2O_4 \cdot H_2O$/KBr heated at 8.15°C $min^{-1}$. The Raman experiments utilized pure $CaC_2O_4 \cdot H_2O$ in a packed capillary tube; this work and others [26] have proven that these differences significantly affect the sample's behavior.

The XRD results showing the relative phase purity of the starting material did not exclude the possible coexistence of the high-temperature form at room temperature: spectroscopic techniques sensitive to the presence of impurity-level quantities of this

phase are necessary to prove that conclusion. XRD patterns of $CaC_2O_4 \cdot H_2O$ at multiple temperatures between 20 and 100°C under both dry and water-vapor-saturated argon atmospheres exhibited no clear phase transitions in this temperature range. These results are shown in Figs. 11 and 12. Fig. 13 shows the five reference XRD patterns for $CaC_2O_4 \cdot H_2O$. Significant changes in the diffraction peaks occur in going from the low- to high-temperature phase(s); it is surprising that our results did not. The only definitive changes in these XRD patterns occured from 85 to 100°C in the dry atmosphere experiments where $\alpha$-$CaC_2O_4$ was formed owing to a shift of the dehydration equilibrium to lower temperature relative to the temperature observed when an atmosphere saturated with water vapor was used.

Thermomechanical analysis results exhibited three major features: an inflection point at 83°C, shrinkage, and then expansion during dehydration. Drastic sample

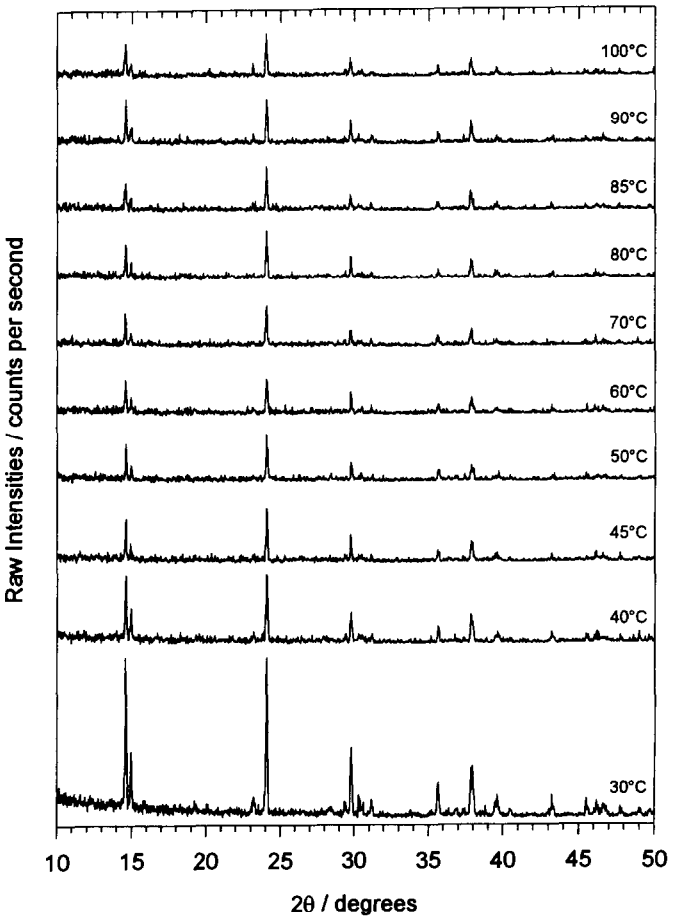


Fig. 11. Isothermal XRD patterns of calcium oxalate monohydrate under dry argon flowing at 20 ml $min^{-1}$ and temperatures from 30 to 100°C.

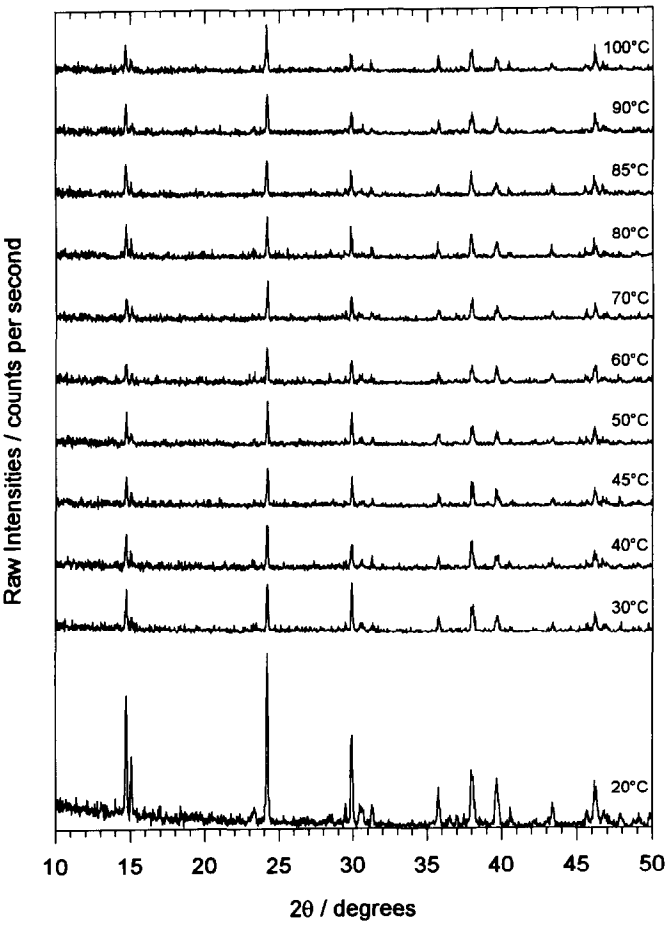


Fig. 12. Isothermal XRD patterns of calcium oxalate monohydrate under an atmosphere of argon saturated with water vapor flowing at 20 ml $min^{-1}$ and temperatures from 20 to 100°C.

decrepitation occurred during the decomposition of calcium oxalate to calcium carbonate (see Fig. 14). The shrinkage of the sample during oxalate to carbonate decomposition was expected and occurred within a reasonable temperature region. The dehydration was similarly expected to result only in shrinkage of the sample, but apparently once the sample's exposed surfaces and regions near the surface dehydrated, the sample began to bloat or foam because the dehydration water molecules could not escape. The trapped molecules became a gas within the powder matrix, effecting a large change in volume. The relative cohesiveness of the sample itself and the low probe load lend further support to this conclusion.

The inflection point in the TMA results at 83°C is magnified in Fig. 15. Inflection points in TMA are associated with structural changes within a sample, usually thermodynamically higher-order phase transitions. Further experiments are necessary,

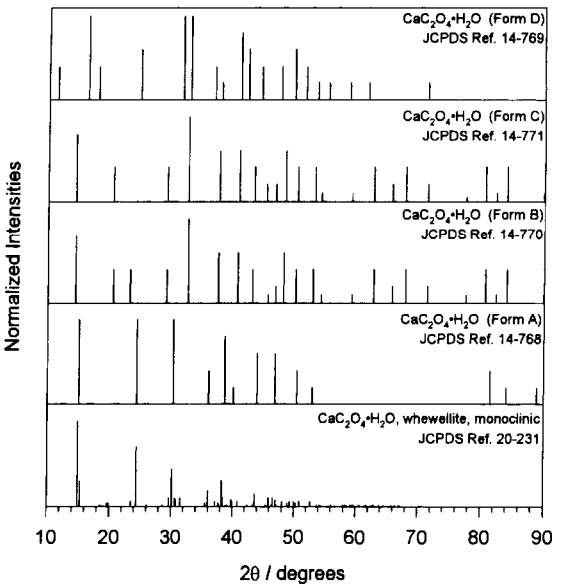


Fig. 13. All JCPDS reference XRD patterns for calcium oxalate monohydrate. (JCPDS reference 20–231 is the generally accepted low-temperature phase, and reference 14–768 is the generally accepted high-temperature phase.)

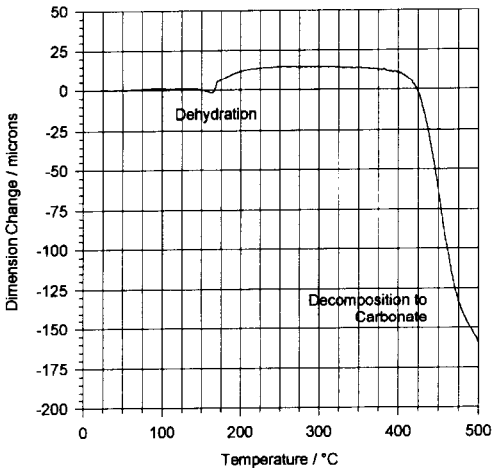


Fig. 14. TMA results for 22.67 mg of calcium oxalate monohydrate loosely packed into an open aluminum pan and heated at 1°C $min^{-1}$ in a furnace open to ambient air.

but the temperature of this inflection point agrees well with the peak maxima temperatures observed in the MDSC™ and DSC results.

The peak observed by MDSC™ and DSC between 65 and 85°C and the TMA inflection point at 83°C may be the completion of the order–disorder transition

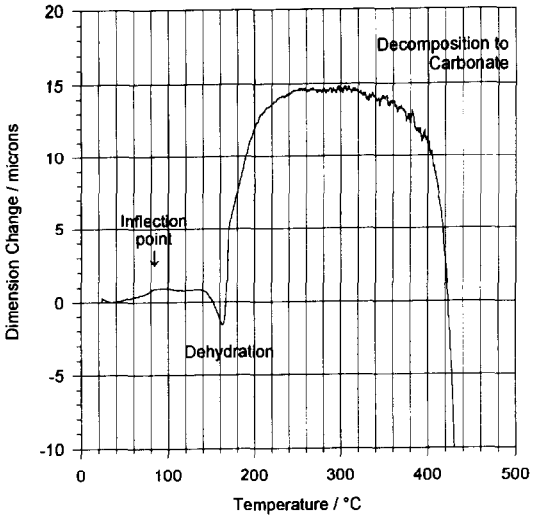


Fig. 15. Expanded Y-axis profile of TMA results for 22.67 mg of calcium oxalate monohydrate loosely packed into an open aluminum pan and heated at 1°C $min^{-1}$ in a furnace open to ambient air.

observed by XRD, Raman and DRIFTS/MS at 45–50°C. Differing experimental conditions in each case may explain the differences in observed completion temperatures. The XRD results used single crystal samples [7]; the XRD patterns and Raman spectra were acquired isothermally. Only the DRIFTS/MS results were obtained in the temperature-scanning mode in the same manner as the MDSC™ and DSC results, but a 100% $CaC_2O_4 \cdot H_2O$ sample was not used. Further, MDSC™ and DSC measure macroscopic changes in heat flow resulting from microscopic changes occurring within a sample. Microscopic changes are the quantities probed by the spectroscopic and diffraction methods mentioned. Finally, the TMA results, another probe of macroscopic properties, appear to better support a bulk structure change of the monohydrate at 83°C than at any other temperature. Thus it seems plausible that these large differences in the observed peak transition temperature originate from fundamental differences between the analytical methods and experimental conditions employed.

## 4. Conclusions

Broadly, dynamic DSC is a powerful tool for identifying thermodynamically higher-order phase transitions, especially those in close proximity to larger enthalpic events. Slow overall heating rates coupled with higher instantaneous heating rates enhance resolution and sensitivity simultaneously. Dynamic DSC also provides consistently high signal-to-noise ratios in reversible heat flow results from liquid nitrogen temperatures to the upper temperature limits of the instrument.

More specifically, calcium oxalate monohydrate exhibits completion of a single thermodynamically higher-order phase transition between 0 and 100°C according to

MDSC™, DSC and TMA results. The temperature associated with the peak maximum of this thermal event varied as a function of heating rate from 65 to 85°C. This temperature range is not in good agreement with previous XRD, Raman and DRIFTS/MS results which reported completion of this transition from 45 to 50°C. This disagreement may be due to differences in sample preparation and/or configuration, sample environment and especially heating rates. The onset temperature of this transition was not discernible in DSC or MDSC™ results. The enthalpy of this transition is about 3 J $g^{-1}$. Polycrystalline XRD results generated under argon atmospheres either dry or saturated with water vapor did not give evidence of any phase transition other than dehydration in the 0–100°C range.

The low- and high-temperature phases of the monohydrate appeared to coexist at temperatures as low as −110°C. A definitive threshold temperature for coexistence of the phases (which necessarily exists but has not been reported previously) was not established; however, the −110 to −70°C range was proposed in this regard. Cooling $CaC_2O_4 \cdot H_2O$ samples to less than −140°C appeared to induce a very small but reproducible endothermic event whose peak temperature decreased according to the lowest temperature which the sample experienced.

## References

[1] D. Duval and R.A. Condrate, Phys. Status Solidi B, 132(1985) 83.
[2] T.A. Shippey, J. Mol. Struct., 63(1980) 157.
[3] Joint Committee for Powder Diffraction Standards (JCPDS) Reference Card Numbers 14–768, 14–769, 14–770, 14–771 and 20–231.
[4] J. Lecomte, Th. Pobequin, J. Wyart, J. Phys. Radium, 6(1945) 22.
[5] deWolff, Technisch. Physiche, Dienst, Delft-Holland. (Author's note: JCPDS card 20–231 provided tabular XRD crystallographic data and this sketchy reference. I did not have access to the article itself).
[6] S. Deganello, News Jahob Miner. Monatsh., (1981) 81.
[7] S. Deganello, Z. Kristallogr., 152(1980) 247.
[8] R. White, Appl. Spectrosc., 46(1) (1992) 93.
[9] R. White, Appl. Spectrosc., 46(10) (1992) 1508.
[10] R. Hocart, G. Watelle-Marion, A. Thrierr-Sorel and N. Gerard, C.R. Acad. Sci., 260(1965) 2509.
[11] S. Schubert and B. Ziemer, Cryst. Res. Tech., 16(9) (1981) 1025.
[12] N. Gerard, N. Wattelle-Marion and A. Thrierr-Sorel, Bull. Soc. Chim., 11(1968) 4367.
[13] M. Mittleman, Thermochim. Acta, 166(1990) 301.
[14] D. Dural and R.A. Condrate, Appl. Spectrosc., 42(1988) 701.
[15] P. Baraldi, Spectrochim. Acta, Part A, 40(1984) 709.
[16] L. Walter-Levy and J. Laniepce, C.R. Acad. Sci., 259(1964) 4685.
[17] D.E. Larkin, ASTM Spec. Tech. Publ., 997(1988) 28.
[18] C.G.R. Nair and K.N. Ninan, Thermochim. Acta, 23(1978) 161.
[19] K.J. Kociba, Master's Thesis, The Ohio State University, 1995 p. 11.
[20] P.S. Gill, S.R. Sauerbrunn and M. Reading, J. Therm. Anal., 40(3) (1993) 931.
[21] N. Buckman, Chem. Aust., 60(12) (1993) 666.
[22] M. Reading, A. Luget and R. Wilson, Thermochim. Acta, 238(1994) 295.
[23] B. Wunderlich, Thermochim. Acta, 238(1994) 287.
[24] W.M. Latimer, P.W. Schutz and J.F.G. Hicks, Jr., Anal. Chem., 55(1933) 971.
[25] R.F. Speyer, Thermal Analysis of Materials, Marcel Dekker New York, 1993.
[26] E.L. Simons and A.E. Newkirk, Talanta, 11(1964) 549.